J. Fluid Mech. (2002), *vol.* 455, *pp.* 347–358.
DOI: 10.1017/S0022112001007492 Printed in the United Kingdom

Very, very fast wetting

By DAVID JACQMIN

NASA Glenn Research Center, Cleveland, OH 44135, USA

(Received 2 September 2001 and in revised form 1 November 2001)

Just after formation, optical fibres are wetted stably with acrylate at capillary numbers routinely exceeding 1000. It is hypothesized that this is possible because of dissolution of air into the liquid coating. A lubrication/boundary integral analysis that includes gas diffusion and solubility is developed. It is applied using conservatively estimated solubility and diffusivity coefficients and solutions are found that are consistent with industry practice and with the hypothesis. The results also agree with the claim of Deneka, Kar & Mensah (1988) that the use of high-solubility gases to bathe a wetting line allows significantly greater wetting speeds. The solutions indicate a maximum speed of wetting which increases with gas solubility and with reduction in wetting-channel diameter.

1. Introduction

Immediately after formation, optical fibres, in order to improve their resilience and refractive properties, are wetted and then coated by running them through a polymer bath. This wetting typically takes place at capillary numbers $Ca = U_0\mu_l/\sigma$ of $O(1000)$, that is, at wetting speeds U_0 of about 1000 to 2000 cm s^{-1}, surface tensions σ of about 20 to 30 dyn cm^{-1}, and liquid viscosities μ_l of about 20 to 40 P (Dimitropoulos *et al.* 2000; Ravinutala *et al.* 2000; Jochem & Ligt 1985; Lyytikäinen 1998).

Optical fibre wetting is somewhat like plunge-tank wetting; in both the material being wetted is drawn through a surrounding free surface. However, with optical fibres wetting takes place in a very narrow orifice – the entrance channel or die of the coating apparatus – that is typically only 300 to 600 μm in diameter (Jochem & Ligt 1985; Dimitropoulos *et al.* 2000; Ravinutala *et al.* 2000). The fibre itself has a diameter of about 125 μm. The gap between the fibre and the orifice wall is thus typically about 100 to 300 μm. The drag of the fibre on the liquid is resisted by the application of high pressures that force-feed the liquid up into the orifice. Because of the fibre's high speed and the relatively high viscosity of the fluid, pressure gradients in the entrance channel are on the order of atmospheres per mm. It appears that proper shaping of the inlet directs these pressures to the wetting line so that air entrainment can be resisted.

These high pressure gradients are undoubtedly helpful in resisting air entrainment. The small size and axisymmetry of the fibre may also be helpful. Simpkins & Kuck (2000) reported a critical capillary number (the maximum Ca for successful resistance of air entrainment) of 2.1 for small-diameter fibres entering unpressurized glycerin. By comparison, for flat tapes in plunge-tank experiments critical Ca is less than 1. For pressurized orifices Simpkins & Kuck have been able to observe and photograph successful wetting at Ca greater than 20 (private communication).

However, the success of high-speed optical fibre wetting cannot be entirely explained in terms of global quantities. Because of the high wetting speed the liquid dynamic

contact angle must be at or near 180°. As will be discussed below, the potential exists for very high and destabilizing pressures to be built up in the receding gas phase near the wetting line. Some theory is needed for how these small-scale but very large stresses are relieved or resolved.

A hint of how this is accomplished is given by the frequent practice in the industry of bathing the wetting line with high-solubility gases. The efficacy of this was first claimed in a patent assigned to Corning Glassworks (Deneka, Kar & Mensah 1988). The gas recommended and claimed in the Corning patent was carbon dioxide, which is typically 3 to 5 times as soluble in polymers as is air. Jochem & Ligt (1985) experimented with CCl_2F_2, which is even more soluble in polymers than CO_2, and showed great improvement in coating speed and quality. With CCl_2F_2 they demonstrated bubble-free coating at $1250\,\mathrm{cm\,s^{-1}}$. With air, using the same wetting die, bubble entrainment occurred at $300\,\mathrm{cm\,s^{-1}}$ (Jochem & Ligt 1987).

The hypothesis indicated by these claims and results is that dissolution of gas into the wetting fluid serves to significantly relieve high gas pressures, thereby facilitating high-speed wetting. In order to examine this hypothesis, this paper discusses a combination lubrication/boundary integral analysis that quantifies gas solubility effects. The analysis approximates the dynamic contact angle as 180°, giving a gas column shape that forms a half-cusp between the wall and the liquid.

Gas properties that could have important effects on high-speed wetting stability include (i) viscosity, (ii) compressibility, (iii) solubility in the liquid, (iv) diffusivity in the liquid, (v) slip along the fibre, (vi) Knudsen diffusion of momentum, significant for gas column thickness less than about 300 nm, and (vii) increased local gas solubility when the gas phase is confined to a very small domain (nanoscale). Properties of the liquid phase include (i) viscosity, (ii) surface tension, (iii) van der Waals attractions between the liquid and the solid and (iv) decrease in the surface tension as the liquid aproaches the solid. The main body of this paper considers the first four gas properties and the first two of the liquid. An Appendix briefly discusses the modelling and effects of most of the remaining properties. Also, Jacqmin (2001) gives a more complete description of modelling of the gas phase. All the properties relegated to the Appendix are stabilizing. Their neglect in the main article thus permits a relatively streamlined analysis of the 'worst case'.

In spite of the huge practical and fundamental scientific interest of high-speed wetting, theoretical attempts aimed at understanding it are largely lacking. An early significant result is by Benney & Timson (1980), who derived an eigenfunction solution for 180° wetting of a solid. Their solution gives the height $H(x)$ of the liquid–gas interface (the distance of the interface from the fibre or, equivalently, the gas-column width) as behaving like $|x|^{m+1}$, where m, the eigenvalue, equals $-\arctan(2Ca)/\pi$.† As Ca goes to ∞, m approaches $1/2$ from above. The solution neglects the effect of gas stresses.

There has been more work on free-surface cusp flows (which can be viewed as 'roll-on' liquid–liquid wetting). Joseph *et al.* (1991), showed that these have the same eigenfunction solution as the one found by Benney & Timson (1980). Shortly after, Jeong & Moffatt (1992) derived exact solutions for near-cusp flows using complex-analysis techniques. These solutions also neglect gas and wetting stresses. At micro- and mesoscale distances from the cusp these solutions approximately match to the Benney & Timson eigenfunction. Jeong & Moffatt showed that the coefficient of the eigenfunction is determined by the outer length scale. In their case this scale was

† This corrects a sign error, introduced at their equation (2.12) and carrying on to (3.9).

the depth of a vortex dipole that drove their flow. At the nanoscale their solutions show a slight rounding of the cusp, which eliminates the singularity in surface tension forcing that would otherwise seem to occur (a delta function with amplitude 2σ).

The difficulty with either cusp or roll-on flow is that the pressure in the displaced gas phase can become very high, leading to instabilities and gas entrainment. The gas phase is swept into the cusp region by the movement of the fluid and of the solid being wetted. Since most of the gas has to return, a Poiseuille-like flow is established with pressure gradients like $1/H^2$. If the flow were precisely cusp or roll-on, and if the gas were completely insoluble in the fluid and obeyed the Navier–Stokes equations, then the gas pressure would be fiercely singular; for the Benney & Timson solution it would be like $x^{-(1+2m)}$. This would dwarf the viscous and surface-tension-related stresses in the liquid. Shikhmurzaev (1998) speculated that this problem might be relieved by Knudsen diffusion. However, this also leads to a singularity (like x^{-m}, see Jacqmin 2001). Nor does slip along the wall solve the difficulty, unless slip is also allowed along the liquid–gas interface. Eggers (2001) recently conducted a lubrication/boundary integral analysis of insoluble two-phase cusp flow assuming, following Jeong & Moffatt (1992), that the cusp is actually slightly rounded. He estimated that failure occurs for $\lambda\kappa^{3/4} > r$, where λ is the viscosity ratio $\mu_{\text{gas}}/\mu_{\text{liq}}$, κ is the curvature at the rounded cusp, and r is a to-be-determined $O(1)$ quantity. Since, from Jeong & Moffatt, $\kappa = c_1 \exp(2\pi Ca)$† where c_1 is $O(1)$, the maximum capillary number for cusp stability would be

$$Ca_{\max} \simeq \frac{2}{3\pi} \ln \frac{1}{\lambda} + O(1). \tag{1.1}$$

This is much too low to account for the stability of optical fibre wetting.

Other industrial processes besides optical fibre manufacturing are reported to allow high-Ca coating. For example, curtain coating (where a metered stream of liquid falls from a height above a moving substrate and then coats the substrate) allows wetting up to a Ca of about 10 (Kistler 1993, p. 343). It seems certain that the additional force and pressures associated with the fall of the liquid act to allow the observed higher wetting speed. Recent experiments by Blake, Bracke & Shikhmurzaev (1999) have quantified some aspects of these effects. Kistler (1993, pp. 339–346) gives a thorough review of the various possible macro- and microscale phenomena that may affect air entrainment and wetting stability.

The following first derives, for given $H(x)$, an integro-differential equation for the pressure p_{g} in the gas phase. This uses a lubrication approximation for the gas flow and a Green's function analysis for the diffusion of the gas into the liquid. $H(x)$ is then found in terms of an integral of the stresses on the liquid interface. This part of the analysis is linearized about a flat interface. Since the interfacial stresses can be expressed in terms of H and p_{g} the system of two equations is closed. We find that there are both minimum and maximum speeds for which successful wetting is possible. For high capillary number these cutoff speeds are expressible in terms of a function of two non-dimensional parameters. The equations are applied to the regime typical of optical fibre coating. It is shown that, indeed, gas solubility significantly mitigates gas pressure and that, in agreement with the claim of Deneka *et al.*, the use of higher-solubility gases makes high wetting speeds easier to achieve.

† This uses the definition of Ca employed by Joseph *et al.*, which is the same as used in this paper and 16 times that of Jeong & Moffatt.

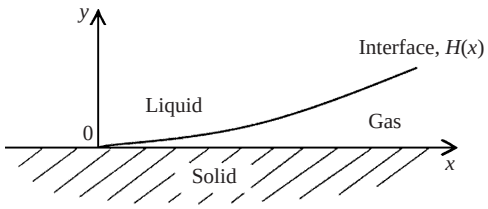

FIGURE 1. The wetting geometry: x is the horizontal coordinate (increasing toward the right), y the vertical. The wetting line is at $x = 0$, $y = 0$. The gas is thus confined to $x > 0$. The solid is moving to the left with velocity $-U_0$.

2. The gas flow

We consider the flow of an isothermal, soluble, ideal gas in a 'half-cusp' region bounded by a solid wall located at $y = 0$ and a liquid interface at $y = H(x)$. The half-cusp is in $x > 0$ and ends at the wetting line at $x = 0$, see figure 1. The bounding surfaces are quasi-parallel, allowing a lubrication flow analysis for the gas. The solid is moving at velocity $-U_0$ and the liquid motion is approximated as also being $-U_0$. The lubrication equations for the gas flow are

$$\frac{\partial u p_g}{\partial x} + \frac{\partial v p_g}{\partial y} = 0, \quad \frac{\partial p_g}{\partial x} = \mu_g \frac{\partial^2 u}{\partial y^2}, \quad p_g = p_g(x), \tag{2.1}$$

where u and v are the gas x- and y-direction velocity components, p_g is the gas pressure, and μ_g is the gas viscosity. The first equation is continuity, the second, x-momentum.

The convection–diffusion equation for the gas in the liquid can be written as

$$-U_0 \frac{\partial C_l}{\partial x} = D\left(\frac{\partial^2 C_l}{\partial x^2} + \frac{\partial^2 C_l}{\partial y^2}\right); \tag{2.2}$$

C_l is the gas concentration in the liquid and D is the diffusivity. C_l is assigned units of pressure.

The boundary conditions at the liquid–gas interface are (i) no-slip, $u = -U_0$, (ii) phase equilibrium, $C_l(H^+) = S p_g(H^-)$, where S is the Henry's law solubility coefficient for the gas in the liquid, and (iii) equality of normal fluxes,

$$-D \left.\frac{\partial C_l}{\partial y}\right|_{H^+} = (v_{gas} - v_{liq}) p_g|_{H^-}.$$

Boundary conditions at the gas–wall interface are (i) no normal velocity and (ii) no-slip. The gas is at atmospheric pressure, designated p_∞, at $x = +\infty$. For simplicity, it will be assumed that the fluid is saturated with the gas (C_l equals S times p_∞) at $x = +\infty$ and $y = +\infty$.

Integration of the continuity equation from 0 to $H(x)$ gives

$$\frac{\partial U_{av} H p_g}{\partial x} = (v_{gas} - v_{interface}) p_g\big|_{H^-} = v_{diffusion}\, p_g\big|_{H^-} = -D \left.\frac{\partial C_l}{\partial y}\right|_{H^+}, \tag{2.3}$$

where $U_{av} = -H^{-1} \int_0^H u \, dy$. From the momentum equation,

$$U_0 - U_{av} = -\frac{1}{\mu_g} \frac{H^2}{12} \frac{\partial p_g}{\partial x}. \tag{2.4}$$

Substituting (2.4) into (2.3) yields

$$\frac{\partial}{\partial x}\left(\frac{H^3}{12\mu_g}p_g\frac{\partial p_g}{\partial x}\right)+\frac{\partial}{\partial x}\left(U_0 H p_g\right)=-D\left.\frac{\partial C_l}{\partial y}\right|_{H^+}. \tag{2.5}$$

In the convection–diffusion equation x-transport is dominated by convection. The x-direction diffusion term can be neglected and the equation reduces to

$$-U_0\frac{\partial C_l}{\partial x}=D\frac{\partial^2 C_l}{\partial y^2}; \tag{2.6}$$

$\partial C_l/\partial y$ also obeys this equation. A Green's function solution is available (Carslaw & Jaeger 1959†) that expresses $\partial C_l/\partial y$ in terms of the boundary values of $\partial^2 C_l/\partial y^2$:

$$\frac{\partial C_l}{\partial y}=-\sqrt{\frac{D}{\pi U_0}}\int_x^\infty \left.\frac{\partial^2 C_l}{\partial y^2}\right|_{y=H^+}\exp\left(-\frac{U_0(y-H)^2}{4D(x'-x)}\right)\frac{\mathrm{d}x'}{\sqrt{x'-x}}. \tag{2.7}$$

This, from (2.6), can be rewritten as

$$\frac{\partial C_l}{\partial y}=\sqrt{\frac{U_0}{\pi D}}\int_x^\infty \left.\frac{\partial C_l}{\partial x'}\right|_{y=H^+}\exp\left(-\frac{U_0(y-H)^2}{4D(x'-x)}\right)\frac{\mathrm{d}x'}{\sqrt{x'-x}}. \tag{2.8}$$

Equation (2.8) can be used to find the flux at the interface in terms of the cusp gas pressure. Multiplying by D, using

$$\left.\frac{\partial C_l}{\partial x'}\right|_{y=H^+}=S\left.\frac{\mathrm{d}p_g}{\mathrm{d}x'}\right|_{y=H^-}$$

and specializing the equation to $y=H^+$ gives

$$D\left.\frac{\partial C_l}{\partial y}\right|_{H^+}=S\sqrt{\frac{DU_0}{\pi}}\int_x^\infty \left.\frac{\mathrm{d}p_g}{\mathrm{d}x'}\right|_{H^-}\frac{\mathrm{d}x'}{\sqrt{x'-x}}. \tag{2.9}$$

Applying this to equation (2.5) then gives

$$\frac{\mathrm{d}}{\mathrm{d}x}\left(\frac{H^3}{12\mu_g}p_g\frac{\mathrm{d}p_g}{\mathrm{d}x}\right)+\frac{\mathrm{d}}{\mathrm{d}x}(U_0 H p_g)=-S\sqrt{\frac{DU_0}{\pi}}\int_x^\infty\frac{\mathrm{d}p_g}{\mathrm{d}x'}\frac{\mathrm{d}x'}{\sqrt{x'-x}}, \tag{2.10}$$

a one-dimensional integro-differential equation for the steady-state pressure of the gas in the half cusp.

3. The liquid flow

The flow in the liquid is taken to be Stokes flow. To leading order its velocity is $-U_0$. Linearizing about $-U_0$ and a flat interface, the kinematic equation for the free surface is

$$-U_0\frac{\partial H}{\partial x}=v_I, \tag{3.1}$$

where v_I is the normal liquid velocity at the interface. This is related to the interfacial stresses by the boundary integral

$$v_I=-\frac{1}{2\pi\mu_l}\int_{-\infty}^{\infty}\ln|x'-x|f_y\,\mathrm{d}x' \tag{3.2}$$

† See equation (9) in § 2.9. The t occurring in the argument of the exponential function should be τ.

(Pozrikidis 1992) where f_y is to first order the interfacial normal stress minus the atmospheric pressure. To this order shear stress contributions to v_I are negligible. Taking the first derivative of (3.2) gives

$$\frac{\partial v_I}{\partial x} = -\frac{1}{2\pi\mu_l}\int_{-\infty}^{\infty}\frac{f_y}{x'-x}\,\mathrm{d}x', \tag{3.3}$$

a Hilbert transform of $f_y/2\mu_l$. It can be inverted to

$$f_y = -\frac{2\mu_l}{\pi}\int_{-\infty}^{\infty}\frac{\partial v_I}{\partial x'}\frac{\mathrm{d}x'}{x'-x} \tag{3.4}$$

and, since v_I in $x<0$ is 0, specialized to

$$f_y = -\frac{2\mu_l}{\pi}\int_{0}^{\infty}\frac{\partial v_I}{\partial x'}\frac{\mathrm{d}x'}{x'-x}; \tag{3.5}$$

$f_y = \sigma H_{xx} + p_g - p_\infty$ and $\partial v_I/\partial x = -U_0 H_{xx}$. Equation (3.5) can thus be arranged in the form of an integral equation for H_{xx} forced by p_g:

$$\sigma H_{xx} - \frac{2\mu_l U_0}{\pi}\int_{0}^{\infty}\frac{H_{x'x'}}{x'-x}\mathrm{d}x' = p_\infty - p_g. \tag{3.6}$$

The equation is linear with a singular Cauchy kernel. The solution for H_{xx}, as discussed by Mikhlin (1957, pp. 126–131), is

$$\frac{\mathrm{d}^2H}{\mathrm{d}x^2} = -\frac{(p_g-p_\infty)/\sigma}{1+4Ca^2} - \frac{2Ca/\pi\sigma}{1+4Ca^2}x^{m-1}\int_{0}^{\infty}\frac{(x')^{1-m}}{x'-x}(p_g(x')-p_\infty)\,\mathrm{d}x' + C_\infty x^{m-1}. \tag{3.7}$$

Equation (3.6) corresponds to Mikhlin's equation (1), p. 127, (3.7) corresponds to his (23). C_∞ is a free parameter. $C_\infty x^{m-1}$, where $m = -\arctan(2Ca)/\pi$, is the homogenous solution to the unforced problem. It is the eigenfunction first found by Benney & Timson. The arctan branch is taken such that m varies from 1 (as $Ca\to 0$) to $1/2$ (as $Ca\to\infty$). This is the only branch that, in equation (3.6), gives a finite integral.

The advantage of equation (3.7) is that $p_g - p_\infty$ is significant only in the microscale region near the wetting line whereas H_{xx} in (3.6) decays very slowly. As $x\to\infty$ the first term on the right-hand side of (3.7) decays like $x^{-(1+2m)}$, the second like x^{m-2} and the eigenfunction term like x^{m-1}. Thus the Benney & Timson eigenfunction becomes dominant and gives the macroscopic shape of the fluid interface. C_∞ is therefore the parameter that allows connection of the macroscale appearance of the flow to its microscale behaviour. Ultimately, as discussed by Jeong & Moffatt (1992, p. 11, their variable $\bar{c}$), its value is related to the outer length scale set by the flow geometry. Since p_g is non-singular, H_{xx} also behaves like x^{m-1} as $x\to 0$. The coefficient of x^{m-1} there is

$$C_0 = C_\infty - \frac{2Ca/\pi\sigma}{1+4Ca^2}\int_{0}^{\infty}(x')^{-m}(p_g(x')-p_\infty)\,\mathrm{d}x'. \tag{3.8}$$

4. The dimensional equations; ranges of parameters

The coupled system of integro-differential equations is thus

$$\frac{\mathrm{d}}{\mathrm{d}x}\left(\frac{H^3}{12\mu_g}p_g\frac{\mathrm{d}p_g}{\mathrm{d}x}\right) + \frac{\mathrm{d}}{\mathrm{d}x}(U_0 H p_g) = -S\sqrt{\frac{DU_0}{\pi}}\int_{x}^{\infty}\frac{\mathrm{d}p_g}{\mathrm{d}x'}\frac{\mathrm{d}x'}{\sqrt{x'-x}}, \tag{4.1}$$

$$\frac{\mathrm{d}^2H}{\mathrm{d}x^2} = -\frac{(p_\mathrm{g}-p_\infty)/\sigma}{1+4Ca^2} - \frac{2Ca/\pi\sigma}{1+4Ca^2}x^{m-1}\int_0^\infty \frac{(x')^{1-m}}{x'-x}(p_\mathrm{g}(x')-p_\infty)\,\mathrm{d}x' + C_\infty x^{m-1}. \quad (4.2)$$

The boundary conditions for the equations are that p_g is finite and $H = H_x = 0$ at $x = 0$ and that p_g equals p_∞ at $x = \infty$. The far-field behaviour of p_g is

$$\frac{\mathrm{d}p_\mathrm{g}}{\mathrm{d}x} \simeq -\frac{12\mu_\mathrm{g}U_0}{H^2} + \frac{12\mu_\mathrm{g}}{H^3 p_\mathrm{g}}L, \quad (4.3)$$

where L is the total rate of dissolution of air into the fluid, the integral from 0 to ∞ of the right-hand-side term in (4.1). It is found as part of the solution. The integral from 0 to ∞ of the first two terms of equation (4.2) is precisely 0. (This result can be shown by converting the integral in x in the second term to a Mellin transform in x/x'.) Because of this the leading-order behaviour of H at ∞ is of the form $C_\infty x^{m+1}/m(m+1)$ plus a constant times x^m.

The equations have seven independent parameters, U_0, μ_g, p_∞, $S\sqrt{D}$, σ, μ_l (in Ca), and C_∞. We are primarily interested in the effects of varying S, C_∞, and U_0. In optical fibre coating the other parameters show less significant variation. A single set of representative values of μ_g, μ_l, D, σ, and p_∞ has therefore been used for all dimensional calculations. In c.g.s. units, this set is $\mu_\mathrm{g} = 0.00019\,\mathrm{P}$, $\mu_\mathrm{l} = 30\,\mathrm{P}$, $D = 0.00003\,\mathrm{cm^2\,s^{-1}}$, $\sigma = 30\,\mathrm{dyn\,cm^{-1}}$, and $p_\infty = 1.01\times10^6\,\mathrm{dyn\,cm^{-2}}$ (one atmosphere). Durrill & Griskey (1966, 1969) give D for a number of different gases diffusing in various molten polymers. The value chosen for these calculations is in the middle range of their data.

Durrill & Griskey also give gas solubilities. From them, carbon dioxide is typically about 4 times as soluble in molten polymers as is air. A typical value of S for air is about 0.1, for CO_2 about 0.4.† Both cases will be considered.

Following the results of Jeong & Moffatt (1992), it will be assumed that C_∞ is approximately equal to the inverse square-root of the length scale of the outer geometry. In their case the outer length scale is vortex dipole depth d and they find a C_∞ of $1.225/\sqrt{d}$. The relevant outer length scale for optical fibre wetting is the gap between the optical fibre and the wetting-channel wall. This is typically 100–300 μm, indicating a range for C_∞ of about 5 to 10.

Optical fibre coating speeds mentioned in the patent literature range from about $300\,\mathrm{cm\,s^{-1}}$ to over 2000. Corresponding capillary numbers range from over 100 to over 2000. The industry norm is in about the middle of this range. These very high capillary numbers will allow some useful simplification of the analysis.

5. Existence of solutions

To be physically valid, solutions for H must be positive, but p_g, which is also necessarily positive, tends to make H_{xx} and thus H negative. At the wetting line, negative H_{xx} would immediately cause H to be negative. C_0 must therefore be greater than 0 and so, from (3.8), it must be true that

$$C_\infty > \frac{2Ca/\pi\sigma}{1+4Ca^2}\int_0^\infty (x')^{-m}(p_\mathrm{g}(x')-p_\infty)\,\mathrm{d}x'. \quad (5.1)$$

For large Ca, a cutoff value of C_∞ exists below which there is no solution. This value is a function of the seven equation parameters.

† This paper uses a somewhat different definition of the coefficient, gas density in the polymer divided by the density of the gas, than do Durrill & Griskey. This increases the coefficients given by Durrill & Griskey by a factor of about 1.6.

At large Ca, for given μ_g, p_∞, $S\sqrt{D}$, σ, μ_l, and C_∞, there can be either no U_0 that allows solutions or a range of solutions from a minimum U_0 (a lower U_0 cutoff) to a maximum (the upper cutoff). Solutions also exist as $Ca \to 0$ in a small region near and below $Ca = 1$.

A simple class of solutions exists for large enough C_∞. If H were of the form αx^β then the shape of p_g and its maximum value would be independent of α. This is because α can then be transformed out of (4.1) by the substitution $x \to \alpha^{-1/(2\beta-1)}x$. At large C_∞, H approximates this form because the third term on the right-hand side of (4.2) dominates the first two. As $C_\infty \to \infty$ the first two terms on the right-hand side of (4.2) stay finite and become independent of C_∞. Equations (4.1) and (4.2) thus partially decouple.

The lower U_0 cutoff occurs where $p_g - p_\infty$ is small but at high enough velocity so that the coefficient of the integral in (4.2) is still $O(1/U_0)$. At small $p_g - p_\infty$ (4.1) can be simplified to

$$\frac{\mathrm{d}}{\mathrm{d}x}\left(\frac{H^3}{12\mu_g}\frac{\mathrm{d}p_g}{\mathrm{d}x}\right) + \frac{\mathrm{d}}{\mathrm{d}x}(U_0 H) = -\frac{S}{p_\infty}\sqrt{\frac{DU_0}{\pi}}\int_x^\infty \frac{\mathrm{d}p_g}{\mathrm{d}x'}\frac{\mathrm{d}x'}{\sqrt{x'-x}}. \tag{5.2}$$

Scaling H like $C_\infty L_s^{m+1}$, where L_s is the inner length scale, and finding L_s by balancing the first and third terms in (5.2), and then the pressure scale p_s by balancing the second and third, one finds that $p_g - p_\infty$ scales like $U_0^{2/3}$. The integral term in (4.2) scales like $(p_g - p_\infty)/U_0$ and therefore like $U_0^{-1/3}$, thus indicating the cutoff. The essential point is that the cutoff occurs in a region where a diminishment in U_0 causes a less rapid diminishment in pressure forcing and so, see (3.6) with the comparatively small σH_{xx} term neglected, the perturbation to H caused by the pressure forcing increases.

6. Non-dimensionalization; specialization to $Ca \gg 1$

The seven parameters can be reduced to three through non-dimensionalization. Setting

$$x \to L_s\hat{x}, \quad H \to C_\infty L_s^{m+1}\hat{H}, \quad p_g \to p_s\hat{p}_g, \tag{6.1}$$

where

$$L_s^{m+1/2} = \frac{S}{C_\infty}\sqrt{\frac{D}{U_0}}, \quad p_s = \frac{\mu_g U_0^2}{S^2 D}, \tag{6.2}$$

(4.1)–(4.2) become

$$\frac{\mathrm{d}}{\mathrm{d}\hat{x}}\left(\frac{\hat{H}^3}{12}\hat{p}_g\frac{\mathrm{d}\hat{p}_g}{\mathrm{d}\hat{x}}\right) + \frac{\mathrm{d}}{\mathrm{d}\hat{x}}\left(\hat{H}\hat{p}_g\right) = -\frac{1}{\sqrt{\pi}}\int_{\hat{x}}^\infty \frac{\mathrm{d}\hat{p}_g}{\mathrm{d}\hat{x}'}\frac{\mathrm{d}\hat{x}'}{\sqrt{\hat{x}'-\hat{x}}}, \tag{6.3}$$

$$\frac{\mathrm{d}^2\hat{H}}{\mathrm{d}\hat{x}^2} = -\frac{\Gamma\left(\hat{p}_g - p_\infty/p_s\right)}{1+4Ca^2} - \frac{2\Gamma Ca/\pi}{1+4Ca^2}\hat{x}^{m-1}\int_0^\infty \frac{(\hat{x}')^{1-m}}{\hat{x}'-\hat{x}}\left(\hat{p}_g(\hat{x}') - \frac{p_\infty}{p_s}\right)\mathrm{d}\hat{x}' + \hat{x}^{m-1}. \tag{6.4}$$

The resulting non-dimensional parameters are Ca, p_∞/p_s and $\Gamma = p_s/\sigma C_\infty L_s^{m-1}$. The boundary condition for $\hat{p}_g$ at $\hat{x} = +\infty$ becomes that $\hat{p}_g$ approaches p_∞/p_s. Since C_∞ has been transformed to 1 the problem of finding its cutoff value has been changed to finding the boundary of the region in $(Ca, p_\infty/p_s, \Gamma)$ for which solutions exist.

As $Ca \to \infty$, $m \to 1/2$ and the length scale L_s becomes $(S/C_\infty)\sqrt{D/U_0}$. The first

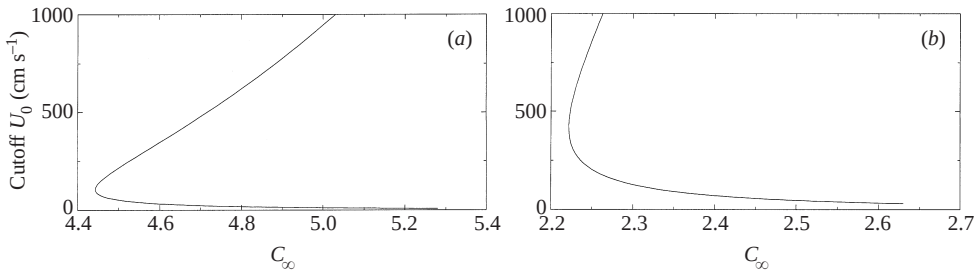

FIGURE 2. Cutoff values of U_0 as a function of C_∞, (*a*) for air with $S = 0.1$; (*b*) for CO_2 with $S = 0.4$. $\mu_g = 0.00019$ P, $\mu_l = 30$ P, $D = 0.00003\,\mathrm{cm^2\,s^{-1}}$, $\sigma = 30\,\mathrm{dyn\,cm^{-1}}$, and $p_\infty = 1.01 \times 10^6\,\mathrm{dyn\,cm^{-2}}$.

$S^2Dp_\infty/\mu_g U_0^2$	10^{-5}	10^{-4}	10^{-3}	10^{-2}	0.1	1.0	10	100
$(\mu_g/2\pi\mu_l)(U_0/C_\infty^2 S^2 D)^{3/4}$	4.560	2.531	1.361	0.687	0.314	0.129	0.048	0.016

TABLE 1. Cutoff values of $(\mu_g/2\pi\mu_l)(U_0/C_\infty^2 S^2 D)^{3/4}$ for given $S^2Dp_\infty/\mu_g U_0^2$.

term on the right-hand side of (6.4) is $O(1/Ca)$ compared to the second and can be neglected. Equation (6.4) reduces to

$$\frac{\mathrm{d}^2\hat{H}}{\mathrm{d}\hat{x}^2} = -\frac{1}{2\pi}\frac{\mu_g}{\mu_l}\left(\frac{U_0}{C_\infty^2 S^2 D}\right)^{3/4}\hat{x}^{-1/2}\int_0^\infty \frac{(\hat{x}')^{1/2}}{\hat{x}'-\hat{x}}\left(\hat{p}_g(x') - \frac{p_\infty}{p_s}\right)\mathrm{d}\hat{x}' + \hat{x}^{-1/2}, \qquad (6.5)$$

while (6.3) remains the same. The number of non-dimensional parameters in the equations has been reduced to two, $(\mu_g/2\pi\mu_l)(U_0/C_\infty^2 S^2 D)^{3/4}$ and $p_\infty/p_s = S^2Dp_\infty/\mu_g U_0^2$. Finding the solution region is now a matter of finding the cutoff value of the first parameter as a function of the second.

7. Results

The equations have been solved numerically using spatially varying node-point separations. For dimensional calculations, grid spacing was typically set to nanometer lengths near the wetting line, up to micron lengths in the outer region. A similar variation in spacing was used for non-dimensional calculations. The derivatives in (4.1) were discretized using central differences. Its integral was solved by approximating $\mathrm{d}p_g/\mathrm{d}x'$ as piecewise constant. The result can be integrated analytically. The integral in (4.2) was approximated by taking $(p_g(x') - p_\infty)(x')^{1-m}$ as piecewise linear. The resulting integrand is then also analytically integrable. Convergence checks were carried out by varying the number of points, grid-stretching parameters, and the length of the calculated region. The numerical solution at the outer calculated point was fitted to the analytic far-field solution. Equation (4.1) can display singular behaviour at $x = 0$. This was avoided by solving it iteratively using a time-like approach. A $\partial p_g/\partial t$-like term was placed on the left-hand side. The second derivative then acts like a diffusion operator and convergence to a finite solution is obtained without much difficulty.

Table 1 gives calculated cutoff values of $(\mu_g/2\pi\mu_l)(U_0/C_\infty^2 S^2 D)^{3/4}$ as a function of $S^2Dp_\infty/\mu_g U_0^2$. The relationship between the two is approximated well by $s = -0.89 - 0.41r - 0.023r^2$, where s and r are logs to the base 10 of the two variables. Figures 2(*a*) and 2(*b*) give some dimensional results drawn from this approximation. They show cutoff values of U_0 as a function of C_∞ for air and for CO_2. The region

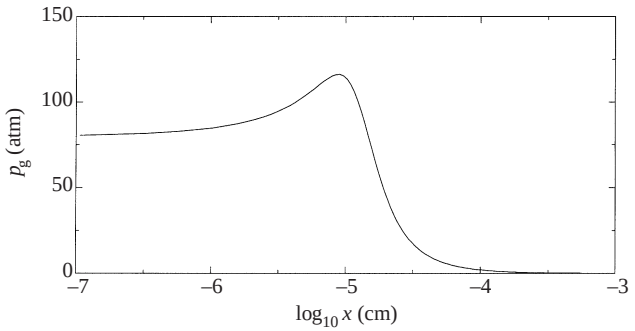

FIGURE 3. Gas pressure as a function of x for air with $U_0 = 1000\ \mathrm{cm\,s^{-1}}$, $C_\infty = 5.3$.

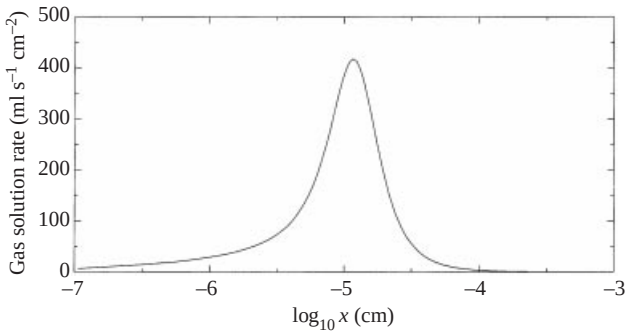

FIGURE 4. Gas solution rate as a function of x for air with $U_0 = 1000\ \mathrm{cm\,s^{-1}}$, $C_\infty = 5.3$. Gas volume as would be measured at standard temperature and pressure.

of existence of solutions is between the upper and lower cutoffs. The values of μ_g, μ_l, D, σ and p_∞ that are used are given in § 4. The minimum value of C_∞ for CO_2 is 2.23, with U_0 equalling $508\ \mathrm{cm\,s^{-1}}$. The minimum value of C_∞ for air is 4.47, with U_0 of 116.

Dimensonal calculations were also made. Of prime interest is maximum pressure developed, to check on the assumptions of gas ideality and Henry's Law, and amount of gas absorbed by the liquid, to check on the possibility of later nucleation of bubbles. Calculations were made for $U_0 = 1000\,\mathrm{cm\,s^{-1}}$ for C_∞ equal to 6, 8 and 10. Using air, the maximum gas pressure developed is, respectively, 147, 181 and 196 atmospheres. The region of high pressure is small; for $C_\infty = 6$, for example, $p_g > 100$ atmospheres extends to only 75 nm from the wetting line, $p_g > 10$ extends to about 300 nm, and $p_g > 2$ extends to about 1.2 μm. The maximum pressure *decreases* as C_∞ approaches cutoff, because of elongation of the air half-cusp and the resulting increase in liquid surface area that the gas can dissolve into. Consistent with this, the volume flux of air into the coating decreases with increasing C_∞; it is $6.8\,\mu\mathrm{l\,s^{-1}\,cm^{-1}}$ (in the direction perpendicular to x and y) for $C_\infty = 6$, 5.9 for $C_\infty = 8$ and 5.3 for $C_\infty = 10$ (volumes at atmospheric pressure and 20 °C). Since the fibre is moving at $1000\,\mathrm{cm\,s^{-1}}$ this is equivalent to absorbing a layer of air only 53 to 68 nm thick. If there is later nucleation of bubbles they would be nanoscopic in scale.

The same calculations for CO_2 yield 30.7, 31.8 and 32.3 atmospheres, with CO_2 fluxes into the coating of 7.74, 6.67 and $5.95\,\mu\mathrm{l\,s^{-1}\,cm^{-1}}$. The case $C_\infty = 4$ gives a maximum pressure of 28.2 and a flux of 9.58. The use of CO_2 instead of air greatly lessens the maximum gas pressure and allows a much smaller C_∞.

Figures 3 and 4 show pressure and gas solution rate as functions of x. The

calculation is for air with $U_0 = 1000\,\mathrm{cm\,s^{-1}}$ and $C_\infty = 5.3$. The flow is close to the cutoff point. Of interest is that the pressure reaches a maximum away from the wetting line. The rate of dissolution is also a maximum there. Very near the wetting line the gas flow is determined by a balance between the second term in (4.1) and its integral. The gas in this region is in nearly plug flow.

8. Conclusions

This paper has attempted to explain the phenomenon of very high capillary number wetting that is common in the optical fibre coating industry. The usual model of wetting, in which the two fluid phases are completely insoluble, points inevitably to wetting failure at an $O(1)$ capillary number (Eggers 2001). However, standard practice in the optical fibre industry is to wet and coat fibres at $Ca = O(1000)$. It has been proposed here that stresses in the receding gas phase that would otherwise be destabilizing are significantly ameliorated by solution of the gas into the wetting liquid. The resulting model of wetting dynamics yields an adjustable macroscopic parameter that has a cutoff value below which there can be no solution. The calculated value of this cutoff is consistent with common practice in the sizing of optical-fibre-coating entrance dies. Maximum and minimum wetting speeds have been found as a function of gas and liquid properties and wetting-channel size. Results indicate that reduction in wetting-channel diameter allows higher wetting speeds. Results also agree with the claim (Deneka *et al.* 1988) that it can be very advantageous to bathe a wetting line with high-solubility gases.

I am very grateful to Dr. Enrique Ramé of the National Center of Microgravity Research for his help and for many interesting and useful discussions.

Appendix. Slip, Knudsen diffusion, and van der Waals forces

Slip and Knudsen diffusion effects are discussed in Jacqmin (2001). With wall slip, equation (2.4) becomes

$$U_0 - U_{\mathrm{av}} = -\frac{1}{\mu_{\mathrm{g}}}\frac{H^2}{2}\left(\frac{1}{2}\frac{H}{H+\lambda} + \frac{\lambda}{H+\lambda} - \frac{1}{3}\right)\frac{\partial p_{\mathrm{g}}}{\partial x}. \tag{A 1}$$

The wall slip length λ is roughly equal to the mean free path. This is about 70 nm at standard temperature and pressure and is proportional to $1/p_{\mathrm{g}}$. There is no slip along the liquid (the two fluids intermingle) and so $U_0 - U_{\mathrm{av}}$ continues to be proportional to $H^2\,\partial p_{\mathrm{g}}/\partial x$. Flux due to Knudsen diffusion, which becomes important below about $H = 5\lambda$, is proportional to $H\partial p_{\mathrm{g}}/\partial x$. Both effects produce a significant amelioration of stresses in the gas. The reduction in maximum pressure is over 50%. This results in turn in about a 50% reduction in gas absorption by the liquid.

Van der Waals forces are normal to the interface and thus can be included in the model analysis. From Israelachvili (1991), the van der Waals forces are equal to the rate of change with H of the sum of the liquid and solid surface tensions (the excess free energies). They can be expressed in the form

$$F = -\frac{A}{6\pi}\frac{H}{(H+H_0)^4} = -\left(\frac{\mathrm{d}\sigma_{\mathrm{L}}}{\mathrm{d}H} + \frac{\mathrm{d}\sigma_{\mathrm{S}}}{\mathrm{d}H}\right). \tag{A 2}$$

For non-polar liquids H_0 should be set to 1.65 Å (Israelachvili 1991). When H is greater than about 1 nm F can be set to the more common form $-A/6\pi H^3$. A is

the Hamaker constant. The actual change in surface tensions (as against the first derivative of their change) becomes important only very close to the wetting line; for H equal to 1 nm, σ_L is still about 97% of its value at ∞.

Calculations have been performed including both van der Waals forces and surface tension variation. The variation in surface tension turns out to be unimportant. Van der Waals attractions are stabilizing, partly in the same way as is large C_∞, in that they cause an increase in H_x in the vicinity of the wetting line. They also, of course, resist the gas pressure. The importance of this is currently under study. Early results suggest that van der Waals forces may operate at too small a length scale to play a major role in setting either interface shape or the cutoff value of C_∞.

REFERENCES

Benney, D. J. & Timson, W. J. 1980 The rolling motion of a viscous fluid on and off a rigid surface. *Stud. App. Maths* **63**, 93–98.

Blake, T. D., Bracke, M. & Shikhmurzaev, Y. D. 1999 Experimental evidence of nonlocal hydrodynamic influence on the dynamic contact angle. *Phys. Fluids* **11**, 1995–2007.

Carslaw, H. S. & Jaeger, J. C. 1959 *Conduction of Heat in Solids*. Oxford University Press.

Deneka, C. W., Kar, G. & Mensah, T. O. 1988 Method for coating optical waveguide fiber. US Patent 4,792,347.

Dimitropoulos, C., Chippada, S., Grald, E. & Kulkarni, J. 2000 CFD Simulation of optical fiber coating flows. *Proc. 49th Intl Wire and Cable Symp.*

Durrill, P. L. & Griskey, R. G. 1966 Diffusion and solution of gases in thermally softened or molten polymers, Part I. *AIChE J.* **12**, 1147–1151.

Durrill, P. L. & Griskey, R. G. 1969 Diffusion and solution of gases in thermally softened or molten polymers, Part II. *AIChE J.* **15**, 106–110.

Eggers, J. 2001 Air entrainment through free surface cusps. *Phys. Rev. Lett.* **86**, 4290–4293.

Israelachvili, J. 1991 *Intermolecular and Surface Forces*. Academic Press.

Jacqmin, D. 2001 Very fast wetting in the presence of soluble gases. In *Proc. IUTAM Symp. on Free Surface Flows* (ed. Y. D. Shikhmurzaev), pp. 134–151. Kluwer.

Jeong, Jae-Tack & Moffatt, H. K. 1992 Free-surface cusps associated with flow at low Reynolds number. *J. Fluid Mech.* **241**, 1–22.

Jochem, C. M. G. & van der Ligt, J. W. C. 1985 Method for cooling and bubble-free coating of optical fibres at high drawing rates. *Electronics Lett.* **21**, 786–787.

Jochem, C. M. G. & van der Ligt, J. W. C. 1987 Method of and arrangement for coating a fibre. US Patent 4,704,307.

Joseph, D. D., Nelson, J., Renardy, M. & Renardy, Y. 1991 Two-dimensional cusped interfaces. *J. Fluid Mech.* **223**, 383–409.

Kistler, S. F. 1993 Hydrodynamics of wetting. In *Wettability* (ed. J. Berg), pp. 311–429. Marcel Dekker.

Lyytikäinen, K. 1998 Numerical modeling of optical fiber coating process. Report to the European Commission's High Performance Computing and Networking Programme, available at http://www.hpcn-ttn.org/ttn/finalreports/OPTIFIBER.pdf

Mikhlin, S. G. 1957 *Integral Equations*. Pergamon.

Pozrikidis, C. 1992 *Boundary Integral and Singularity Methods for Linearized Viscous Flow*. Cambridge University Press.

Ravinutala, S., Rattan, K., Polymeropoulos, C. & Jaluria, Y. 2000 Dynamic menisci in a pressurized fiber applicator. *Proc. 49th Intl Wire and Cable Symp.*

Shikhmurzaev, Y. D. 1998 On cusped interfaces. *J. Fluid Mech.* **359**, 313–328.

Simpkins, P. G. & Kuck, V. J. 2000 Air entrapment in coatings by way of a tip-streaming meniscus. *Nature* **403**, 641–643.